Green Chemistry

ROYAL SOCIETY OF CHEMISTRY

COMMUNICATION

View Article Online
View Journal | View Issue

Cite this: *Green Chem.*, 2023, **25**, 1326

Received 19th November 2022,
Accepted 26th January 2023

DOI: 10.1039/d2gc04368h

rsc.li/greenchem

Identifying the optimal oxidation state of Cu for electrocatalytic reduction of CO_2 to C_{2+} products†

Liang Xu,[a] Jiaqi Feng,[a] Limin Wu,[a,b] Xinning Song,[a,b] Xingxing Tan,[a,b] Libing Zhang,[a,b] Xiaodong Ma,[a,b] Shunhan Jia,[a,b] Juan Du,[c] Aibing Chen,[c] Xiaofu Sun *[a,b] and Buxing Han *[a,b,d]

The electrocatalytic CO_2 reduction reaction (CO_2RR) to C_{2+} products is of great importance. It is known that the co-operation of Cu^{1+} and Cu^0 in the catalysts can yield a high faradaic efficiency (FE). However, it is very difficult to figure out the optimal ratio of Cu^{1+} and Cu^0 because Cu^{1+} can be reduced to Cu^0 during CO_2RR. To solve this problem and identify the optimal oxidation state of Cu, herein we propose a strategy to prepare Cu catalysts with different oxidation states, which could be stabilized by the pulsed electrolysis method during CO_2RR. On the basis of this method, we have studied the effect of the oxidation state of Cu on CO_2RR to form C_{2+} products. It has been found that the Cu catalyst with an oxidation state of +0.41 is the most efficient in our reaction system, and the FE of C_{2+} products is 70.3% in an H-type cell. This work provides a precise method to identify the optimal oxidation state of the catalysts that are not stable in the reaction.

The electrocatalytic CO_2 reduction reaction (CO_2RR) to form value-added carbon-based chemicals and fuels by utilizing renewable electricity is a promising technology to mitigate CO_2 emissions, fulfil the anthropogenic carbon cycle, and store excess renewable electricity as chemical energy.[1–7] Among the products that can be generated from CO_2RR, C_{2+} products are the most desirable due to their high energy densities and industrial value as chemical feedstocks.[8–12] However, their selectivity and activity are severely limited by multistep hydrogenation and the sluggish kinetics of C–C coupling steps. To date, copper is known to be the most efficient electrocatalyst for selectively converting CO_2 to C_{2+} products.[13–16] The synergism of Cu^{1+} and Cu^0 sites in copper catalysts has been verified to achieve high faradaic efficiency (FE) for CO_2-to-C_{2+} products.[17–20] However, previous research has shown that Cu^{1+} species are reduced to Cu^0 in the reaction.[21–23] Therefore, it is challenging to confirm the optimal Cu oxidation state for efficient electrocatalytic CO_2RR.

Various strategies have been used to tune the Cu electron structure, such as space confinement,[24,25] the synthesis of alloys,[26] doping heteroatoms,[27,28] and organic ligand modification.[29,30] Among these, organic ligand modification (*e.g.* carboxylate and imidazole) has been reported to stabilize metal centers with appropriate oxidation states, and thus affects the intermediate adsorption during CO_2RR.[30–36] Meanwhile, the Cu-based catalyst prepared by modifying the carboxylate ligand showed unique electrochemical CO_2 reduction selectivity toward C_{2+} products.[37–39] This has made the method to be viewed as a good candidate for constructing Cu^{1+} catalytic sites to promote the formation of C_{2+} products. However, the content of Cu^{1+} drops dramatically during the potentiostatic electrolysis, resulting in the change of CO_2RR catalytic activity.

Pulsed potential electrolysis has emerged as a simple and effective method to increase the reaction durability and improve the product selectivity in CO_2RR *via* tuning the surface architecture, oxidation state, surface adsorbate coverage and local pH.[40–44] Meanwhile, the pulsed electrochemical method is also a simple and quick method to prepare various materials, such as metals, alloys, metal chalcogenides and porous materials.[45–49] Recently, based on the pulsed electrolysis method, our group proposed the "*in situ* periodic regeneration of catalyst (PR-C)" strategy to give long-term high efficiency of CO_2 electroreduction to generate C_{2+} products over the Cu catalyst by applying a positive potential pulse for a short time periodically in the halide-containing electrolyte.[50] At the same time, we also found that the Cu catalyst could be

[a]*Beijing National Laboratory for Molecular Sciences, CAS Key Laboratory of Colloid and Interface and Thermodynamics, CAS Research/Education Center for Excellence in Molecular Sciences, Institute of Chemistry, Chinese Academy of Sciences, Beijing 100190, China. E-mail: sunxiaofu@iccas.ac.cn, hanbx@iccas.ac.cn*
[b]*School of Chemical Sciences, University of Chinese Academy of Sciences, Beijing 100049, China*
[c]*College of Chemical and Pharmaceutical Engineering, Hebei University of Science and Technology, Shijiazhuang 050018, China*
[d]*Shanghai Key Laboratory of Green Chemistry and Chemical Processes, School of Chemistry and Molecular Engineering, East China Normal University, Shanghai 200062, China*

† Electronic supplementary information (ESI) available. See DOI: https://doi.org/10.1039/d2gc04368h

in situ regenerated to maintain the stability of the oxidation state of Cu *via* the pulsed potential electrocatalytic CO_2RR.

Identifying the optimal oxidation state of Cu in CO_2RR to form C_{2+} products is of importance from both fundamental and practical points of views. Herein, we designed and prepared several $Cu_xC_yO_z$ catalysts with different Cu oxidation states using the pulsed electrochemical method. The oxidation state of Cu was stabilized by the pulsed potential in CO_2RR, and the optimal oxidation state of Cu for producing C_{2+} products was figured out. It was found that the catalyst with an average Cu valence state of 0.41 was most efficient, and the FE of C_{2+} products could reach 70.3% with a current density of 24.1 mA cm^{-2} at −1.0 V *versus* the reversible hydrogen electrode (RHE).

As illustrated in Fig. 1A, the catalysts were prepared *via* a pulsed electrochemical method in 0.1 M $KHCO_3$ aqueous electrolyte containing 0.1 M potassium benzenedicarboxylate (K_2BDC). A typical H-type cell with three-electrode configuration was used in this work, which included a Cu foil working electrode, a Pt gauze counter electrode, and an Ag/AgCl reference electrode. Cu^{2+} ions were generated at the anode potential (E_a = 1.25 V *vs.* RHE), and they interacted with negatively charged carboxylate ligands to form the Cu complex. The Cu complex was then reduced to $Cu_xC_yO_z$ at the cathode potential (E_c = −1.0 V *vs.* RHE). Anodic pulses (t_a) of 3 s followed by cathodic pulses (t_c) of 5 s were applied in this work. Such pulses were repeated for 80 cycles.

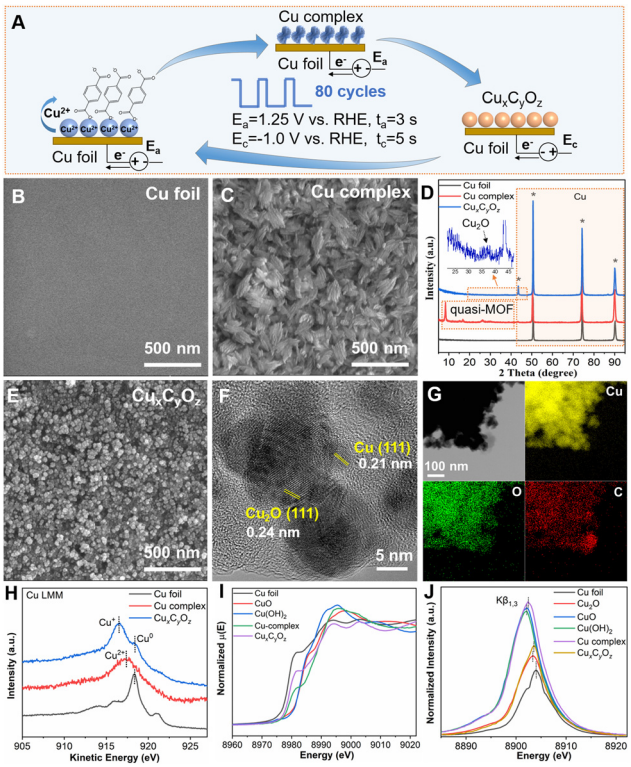

Fig. 1 (A) Schematic diagram of the preparation of the $Cu_xC_yO_z$ catalyst. SEM images of (B) Cu foil, (C) Cu complex, and (E) $Cu_xC_yO_z$. (D) XRD patterns of different samples. (F) HR-TEM image and (G) elemental mappings images of $Cu_xC_yO_z$. (H) The quasi *in situ* XPS signals of Cu Auger LMM spectra for the Cu foil, Cu complex, and $Cu_xC_yO_z$. (I) XANES spectra and (J) XES spectra of different samples.

The scanning electron microscopy (SEM) image showed that the untreated Cu foil had a smooth surface (Fig. 1B). The Cu complex has a leaf-like structure generated by the stacking of lamellae due to the application of E_a (Fig. 1C). The X-ray diffraction (XRD) patterns in Fig. 1D confirmed the presence of a crystalline quasi-metal–organic framework (MOF).[39] After that, the electrochemical reconstruction[51–53] was performed by reducing the Cu complex in an electrolyte to form the $Cu_xC_yO_z$ catalyst. The leaf-like structure was converted into uniform nanoparticles (Fig. 1E). The high-resolution transmission electron microscopy (HR-TEM) image (Fig. 1F) confirmed that both metallic Cu and Cu_2O crystal lattices existed in the $Cu_xC_yO_z$ catalyst, where 0.21 nm and 0.24 nm belong to Cu (111) and Cu_2O(111), respectively.[54,55] This can also be confirmed from the XRD patterns (Fig. 1D). The corresponding energy-dispersive X-ray spectroscopy (EDS) results showed that the atomic ratio of Cu : C : O was approximately 4 : 2 : 1 (Table S1†). The EDS for elemental mapping (Fig. 1G) showed that the Cu, C and O elements were distributed homogeneously throughout the entire architectures.

The surface analysis of different samples was performed by quasi *in situ* X-ray photoelectron spectroscopy (XPS) (Fig. S1† and Fig. 1H). The Cu 2p XPS spectra and Cu Auger $L_3M_{45}M_{45}$ transition indicated that Cu^{2+} was the major species in the Cu complex, while Cu^0 and Cu^{1+} species existed in $Cu_xC_yO_z$. Furthermore, the detailed structural information of Cu was investigated by *in situ* X-ray absorption spectroscopy (XAS) and X-ray emission spectroscopy (XES). As shown in Fig. 1I, Cu K-edge X-ray absorption near-edge spectroscopy (XANES) of the Cu complex exhibited an edge profile similar to that of CuO or $Cu(OH)_2$ in the range from 8960 to 9020 eV, while the spectrum of $Cu_xC_yO_z$ showed a close absorption edge with the Cu foil. These observations indicated that Cu in $Cu_xC_yO_z$ has a lower oxidation state compared with that in the Cu complex. Both the Cu complex and $Cu_xC_yO_z$ presented a characteristic Cu–Cu peak at 2.3 Å and a Cu–O peak at around 1.5 Å in the extended X-ray absorption fine-structure (EXAFS) spectra (Fig. S2†). However, the intensity of the Cu–O peak decreased and the intensity of the Cu–Cu peak increased in $Cu_xC_yO_z$ compared to those of the Cu complex, suggesting that the oxidized copper in the Cu complex was partially reduced during the formation of $Cu_xC_yO_z$. Fig. 1J shows the Cu $K\beta_{1,3}$ XES spectra of the Cu complex and $Cu_xC_yO_z$. When comparing the spectra with those of the reference samples, the *in situ* spectra for the Cu complex lay in between those for the Cu^{2+} and Cu^+ references, whereas in the case of $Cu_xC_yO_z$, the spectra were in between those for Cu^{1+} and Cu^0. Both the XAS and XES results indicated the co-existence of Cu^{1+} and Cu^0 species in $Cu_xC_yO_z$, which is in line with the XPS data.

It is worth noting that application of different E_a values would affect the oxidation state of Cu in the $Cu_xC_yO_z$ catalyst. As shown in Fig. 2A, we prepared a series of catalysts by changing the E_a. The SEM images are shown in Fig. S3,† and their

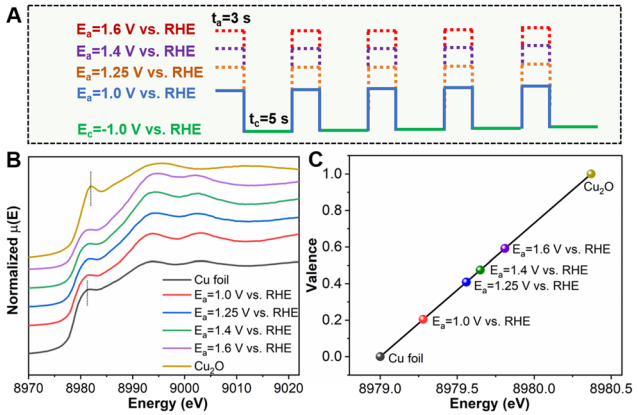

Fig. 2 (A) Schematic diagram of the preparation of the $Cu_xC_yO_z$ catalyst under different conditions (E_a = 1.0 V, 1.25 V, 1.4 V, and 1.6 V *vs.* RHE, t_a = 3 s, E_c = −1.0 V *vs.* RHE, t_c = 5 s). (B) XANES spectra at the Cu K-edge under different conditions. (C) Average oxidation state of Cu in $Cu_xC_yO_z$ under different conditions from Cu K-edge XANES.

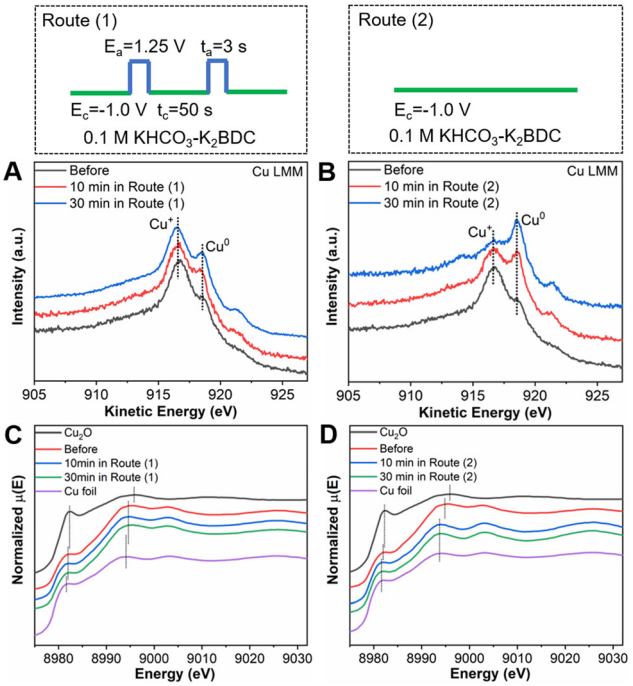

Fig. 3 The quasi *in situ* Auger LMM spectra of Cu for $Cu_xC_yO_z$(0.41) reacted in (A) route (1) and (B) route (2) for different times. The *in situ* XANES spectra of $Cu_xC_yO_z$(0.41) reacted in (C) route (1) and (D) route (2) for different times.

morphologies were quite similar. The impact of the applied E_a on the Cu oxidation state was further investigated using XANES (Fig. 2B). The absorption edges of all the samples reside between those of Cu^0 and Cu^{1+}. We also acquired the oxidation state of Cu as a function of the Cu K-edge energy shift (Fig. 2C). The detailed calculation method for quantifying the oxidation average valence state of Cu is discussed in the ESI (Table S2†). The average valence of Cu increased gradually with the increase of the applied E_a, which was +0.20, +0.41, +0.47 and +0.59, when the applied E_a was 1.0 V, 1.25 V, 1.4 V, and 1.6 V *vs.* RHE, respectively. For making a clear distinction, these $Cu_xC_yO_z$ catalysts with different Cu oxidation states are denoted as $Cu_xC_yO_z$(0.20), $Cu_xC_yO_z$(0.41), $Cu_xC_yO_z$(0.47), and $Cu_xC_yO_z$(0.59).

Next, quasi *in situ* XPS and Auger LMM transition measurements were performed to characterize the composition and structure changes of the catalysts during the CO_2RR in different routes. In route (1), pulsed electrolysis (E_a = 1.25 V *vs.* RHE, t_a = 3 s; E_c = −1.0 V *vs.* RHE, t_c = 50 s) was applied in 0.1 M $KHCO_3$–K_2BDC electrolyte. The same electrolysis conditions as applied for the preparation of $Cu_xC_yO_z$ catalyst were followed for the CO_2RR, except that the time of t_c was extended. In route (2), potentiostatic electrolysis was applied in 0.1 M $KHCO_3$–K_2BDC electrolyte with E_c = −1.0 V *vs.* RHE. As shown in Fig. 3A and B, the content of Cu^{1+} could be maintained unchanged in route (1), while it would be decreased gradually in route (2). To further investigate the changes in the Cu oxidation state, operando XAS at the Cu K-edge was carried out. The Cu K-edge XANES spectra of $Cu_xC_yO_z$(0.41) used in route (1) for different times exhibited an edge profile similar to that of the catalyst before the reaction, while close to the absorption edge of the Cu foil when reacted in route (2) (Fig. 3C and D). On the other hand, the intensity of Cu–Cu coordination (2.3 Å) of $Cu_xC_yO_z$(0.41) in route (1) was basically unchanged compared to that of the catalyst before the reaction, but it gradually increased in route (2) in the Fourier transform (FT) of the EXAFS spectra in *R* space (Fig. S4†). The results demonstrated that the Cu oxidation state can be maintained by the *in situ* regeneration of Cu^+ during the CO_2RR in route (1), while it declined gradually to tend to Cu^0 during the CO_2RR in route (2).

The CO_2RR performances of $Cu_xC_yO_z$ catalysts were then investigated in an H-type cell under different electrolysis conditions for 2 h. We considered the effect of K^+ concentration on the CO_2RR performance, and found that the increase of the K^+ concentration in the electrolyte did not promote the formation of C_{2+} products (Fig. S5†). We also carried out the electrolysis experiments under a N_2 atmosphere (without CO_2). No carbon-based reduction product could be detected, indicating that CO_2 was the carbon source in this work. For $Cu_xC_yO_z$(0.41), it had a higher current density at −0.9 to −1.25 V *vs.* RHE in route (1) than that in route (2) (Fig. 4A and B). Route (1) also showed a significant difference in the distributions of CO_2RR products compared with route (2). C_1 products (CO, formate and methane), C_{2+} products (ethylene, ethanol and *n*-propanol) and H_2 can be detected by ^{1}H nuclear magnetic resonance (NMR) spectroscopy and gas chromatography (GC). The FE for C_{2+} products in route (1) was much higher than that in route (2). In route (1), the $Cu_xC_yO_z$(0.41) catalyst exhibits a volcano-shaped dependence of total FE for C_{2+} products at different E_c values, and the maximum FE (C_{2+} products) could reach up to 70.3% at −1.0 V *vs.* RHE with a current density of 24.1 mA cm^{-2}, while the highest FE for C_{2+} products was only 46.6% in route (2). The catalyst also showed

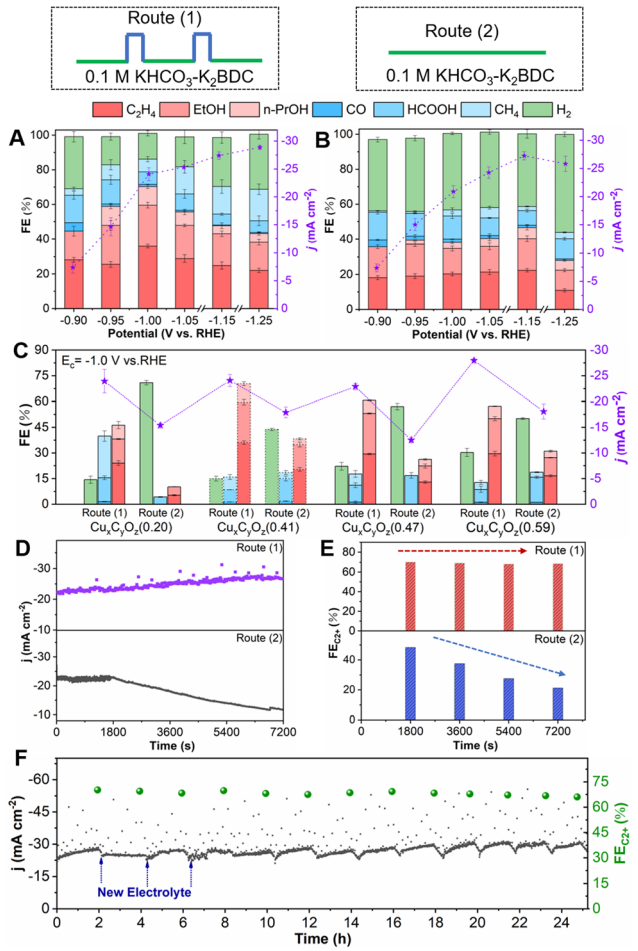

Fig. 4 CO_2RR product distribution and current density (j) of $Cu_xC_yO_z$(0.41) in (A) route (1) and (B) route (2). (C) CO_2RR product distribution and current density of $Cu_xC_yO_z$ with different oxidation states of Cu. (D and E) Dependence of the current density (j) and FE of $Cu_xC_yO_z$(0.41) on time in route (1) and route (2). (F) Long-term stability of CO_2 pulsed electroreduction over $Cu_xC_yO_z$(0.41).

lower CO_2RR performance to form C_{2+} products in routes (3) and (4) in 0.1 M $KHCO_3$ (Fig. S6†).

Furthermore, the CO_2RR performance of other $Cu_xC_yO_z$ catalysts was also evaluated. The $Cu_xC_yO_z$(0.41) catalyst exhibited an optimal CO_2-to-C_{2+} product performance with the average Cu valence state of 0.41 under an E_a of 1.25 V (Fig. 4C). In the control experiments, we optimized the duration of the pulse (t_a and t_c) and the concentration of the electrolyte. The detailed discussion is shown in the ESI (Fig. S7–S12†). The final optimized reaction conditions are E_a = 1.25 V *vs.* RHE, t_a = 3 s, E_c = −1.0 V *vs.* RHE, t_c = 50 s, and the FE of C_{2+} products was the highest in the electrolyte containing 0.1 M K_2BDC.

Based on the above analysis, some important observations are summarized below.

(1) The pulsed electrolysis can effectively inhibit the hydrogen evolution reaction (HER) and promote the formation of C_{2+} products.

(2) The addition of K_2BDC in the electrolyte did not contribute to the formation of C_{2+} products by comparing to that in routes (2) and (4) under potentiostatic electrolysis conditions (Fig. 4B and Fig. S6B†), while the addition of K_2BDC in the electrolyte combined with pulsed electrolysis can achieve the *in situ* regeneration of the $Cu_xC_yO_z$ catalyst to stabilize the oxidation state of Cu during the pulsed CO_2RR, leading to the improved CO_2-to-C_{2+} performance.

(3) The oxidation state of Cu in $Cu_xC_yO_z$ catalysts could regulate the CO_2-to-C_{2+} product performance. The optimal oxidation state of Cu in $Cu_xC_yO_z$ catalysts was +0.41 corresponding to the best CO_2-to-C_{2+} performance.

(4) The SEM images show that there was no obvious change after different reaction times in route (1) and route (2) (Fig. S13†), suggesting that the K_2BDC in the electrolyte did not change the morphology of the catalyst, which also confirmed that the change in CO_2RR performance did not originate from the variation of the catalyst morphology.

The stability was crucial for the application of CO_2RR. First, the current density of CO_2RR and the FE of C_{2+} products, which depend on the reaction time within 2 h, were investigated. Obviously, the current density and FE of C_{2+} products over the $Cu_xC_yO_z$(0.41) catalyst did not change significantly with time in route (1), while both of them decreased continuously in route (2) (Fig. 4D and E). The $Cu_xC_yO_z$ catalysts with the other oxidation states of Cu also show a similar phenomenon (Fig. S14†). Furthermore, consecutive cycles were carried out to determine the long-term CO_2RR stability of the $Cu_xC_yO_z$(0.41) catalyst in route (1). The current density and FE of C_{2+} products did not change notably over 25 hours in route (1) (Fig. 4F). The results demonstrated that $Cu_xC_yO_z$(0.41) exhibited outstanding catalytic activity and stability toward CO_2RR in route (1) due to the fact that Cu in the catalyst has an optimal oxidation state and can be maintained by the *in situ* regeneration of Cu during the reaction.

Conclusions

In summary, the $Cu_xC_yO_z$ catalysts with different Cu oxidation states have been synthesized *via* the pulsed electrochemical method. The oxidation state of Cu can be stabilized by the pulsed anode potential in CO_2RR, which allows us to study the effect of the oxidation state of Cu on the performance of the catalysts more precisely. It is found that the FEs of C_{2+} products depend strongly on the oxidation state of Cu. The catalyst with a Cu oxidation state of +0.41 yields the highest C_{2+} FE of 70.3% with a current density of 24.1 mA cm^{-2} in an H-type cell. This work provides a precise method to identify the optimal oxidation state of the catalysts. This method is specifically favorable for studying the catalysts that are not stable during the electrochemical reaction due to the reduction of the active species. Obviously, it is also useful for designing efficient catalysts with a suitable oxidation state for CO_2RR.

Author contributions

L. X., X. F. S. and B. X. H. proposed the project, designed the experiments, and wrote the manuscript. L. X. performed the whole experiments. J. Q. F., L. M. W., X. N. S. and X. X. T. performed the analysis of experimental data. L. B. Z., X. D. M. and S. H. J. conducted a part of the characterization study. J. D. and A. B. C. participated in discussions. X. F. S. and B. X. H. supervised the whole project.

Conflicts of interest

There are no conflicts to declare.

Acknowledgements

The work was supported by the National Natural Science Foundation of China (22002172, 22203099 and 22121002), the Beijing Natural Science Foundation (J210020), the S&T Program of Hebei (B2021208074), the Chinese Academy of Sciences (QYZDY-SSW-SLH013) and the Photon Science Center for Carbon Neutrality. The X-ray absorption spectroscopy measurements were performed at Beamline 4B9A at Beijing Synchrotron Radiation Facility (BSRF). The X-ray emission spectroscopy beam time was granted by Beamline 4W1B of BSRF, Institute of High Energy Physics, Chinese Academy of Sciences. The staff members of 4W1B are acknowledged for their support in measurements and data reduction.

References

1 W. Ma, X. He, W. Wang, S. Xie, Q. Zhang and Y. Wang, *Chem. Soc. Rev.*, 2021, **50**, 12897–12914.
2 R. B. Song, W. Zhu, J. Fu, Y. Chen, L. Liu, J. R. Zhang, Y. Lin and J. J. Zhu, *Adv. Mater.*, 2020, **32**, 1903796.
3 D. Gao, P. Wei, H. Li, L. Lin, G. Wang and X. Bao, *Acta Phys.-Chim. Sin.*, 2021, **37**, 2009021.
4 X. Song, L. Xu, X. Sun and B. Han, *Sci. China: Chem.*, 2023, **66**, 315–323.
5 W. Guo, S. Liu, X. Tan, R. Wu, X. Yan, C. Chen, Q. Zhu, L. Zheng, J. Ma, J. Zhang, Y. Huang, X. Sun and B. Han, *Angew. Chem., Int. Ed.*, 2021, **60**, 21979–21987.
6 J. H. Ye, T. Ju, H. Huang, L. L. Liao and D. G. Yu, *Acc. Chem. Res.*, 2021, **54**, 2518–2531.
7 D. G. Yu and L. N. He, *Green Chem.*, 2021, **23**, 3499–3501.
8 H. L. Zhu, H. Y. Chen, Y. X. Han, Z. H. Zhao, P. Q. Liao and X. M. Chen, *J. Am. Chem. Soc.*, 2022, **144**, 13319–13326.
9 W. Liu, P. Zhai, A. Li, B. Wei, K. Si, Y. Wei, X. Wang, G. Zhu, Q. Chen, X. Gu, R. Zhang, W. Zhou and Y. Gong, *Nat. Commun.*, 2022, **13**, 1877.
10 J. E. Huang, F. Li, A. Ozden, A. S. Rasouli, F. P. García de Arquer, S. Liu, S. Zhang, M. Luo, X. Wang, Y. Lum, Y. Xu, K. Bertens, R. K. Miao, C. T. Dinh, D. Sinton and E. H. Sargent, *Science*, 2021, **372**, 1074–1078.
11 Y. Zhao, X. Zu, R. Chen, X. Li, Y. Jiang, Z. Wang, S. Wang, Y. Wu, Y. Sun and Y. Xie, *J. Am. Chem. Soc.*, 2022, **144**, 10446–10454.
12 X. Yan, C. Chen, Y. Wu, Y. Chen, J. Zhang, R. Feng, J. Zhang and B. Han, *Green Chem.*, 2022, **24**, 1989–1994.
13 Y. Wang, J. Liu and G. Zheng, *Adv. Mater.*, 2021, **33**, 2005798.
14 C. Xiao and J. Zhang, *ACS Nano*, 2021, **15**, 7975–8000.
15 Y. Zhang, P. Li, C. Zhao, G. Zhou, F. Zhou, Q. Zhang, C. Su and Y. Wu, *Sci. Bull.*, 2022, **67**, 1679–1687.
16 C. Liu, J. Gong, Z. Gao, L. Xiao, G. Wang, J. Lu and L. Zhuang, *Sci. China: Chem.*, 2021, **64**, 1660–1678.
17 L. Ding, N. Zhu, Y. Hu, Z. Chen, P. Song, T. Sheng, Z. Wu and Y. Xiong, *Angew. Chem., Int. Ed.*, 2022, **61**, e202209268.
18 T. C. Chou, C. C. Chang, H. L. Yu, W. Y. Yu, C. L. Dong, J. J. Velasco-Vélez, C. H. Chuang, L. C. Chen, J. F. Lee, J. M. Chen and H. L. Wu, *J. Am. Chem. Soc.*, 2020, **142**, 2857–2867.
19 Y. Zhou, Y. Yao, R. Zhao, X. Wang, Z. Fu, D. Wang, H. Wang, L. Zhao, W. Ni, Z. Yang and Y. M. Yan, *Angew. Chem., Int. Ed.*, 2022, **61**, e202205832.
20 J. Wang, H. Y. Tan, Y. Zhu, H. Chu and H. M. Chen, *Angew. Chem., Int. Ed.*, 2021, **60**, 17254–17267.
21 Z. Z. Wu, F. Y. Gao and M. R. Gao, *Energy Environ. Sci.*, 2021, **14**, 1121–1139.
22 S. Popovic, M. Smiljanic, P. Jovanovic, J. Vavra, R. Buonsanti and N. Hodnik, *Angew. Chem., Int. Ed.*, 2020, **59**, 14736–14746.
23 X. Yuan, S. Chen, D. Cheng, L. Li, W. Zhu, D. Zhong, Z. Zhao, J. Li, T. Wang and J. Gong, *Angew. Chem., Int. Ed.*, 2021, **60**, 15344–15347.
24 P. P. Yang, X. L. Zhang, F. Y. Gao, Y. R. Zheng, Z. Z. Niu, X. Yu, R. Liu, Z. Z. Wu, S. Qin, L. P. Chi, Y. Duan, T. Ma, X. S. Zheng, J. F. Zhu, H. J. Wang, M. R. Gao and S. H. Yu, *J. Am. Chem. Soc.*, 2020, **142**, 6400–6408.
25 J. Y. Kim, D. Hong, J. C. Lee, H. G. Kim, S. Lee, S. Shin, B. Kim, H. Lee, M. Kim, J. Oh, G. D. Lee, D. H. Nam and Y. C. Joo, *Nat. Commun.*, 2021, **12**, 3765.
26 F. Hu, L. Yang, Y. Jiang, C. Duan, X. Wang, L. Zeng, X. Lv, D. Duan, Q. Liu, T. Kong, J. Jiang, R. Long and Y. Xiong, *Angew. Chem., Int. Ed.*, 2021, **60**, 26122–26127.
27 W. He, I. Liberman, I. Rozenberg, R. Ifraemov and I. Hod, *Angew. Chem., Int. Ed.*, 2020, **59**, 8262–8269.
28 Z. Yin, C. Yu, Z. Zhao, X. Guo, M. Shen, N. Li, M. Muzzio, J. Li, H. Liu, H. Lin, J. Yin, G. Lu, D. Su and S. Sun, *Nano Lett.*, 2019, **19**, 8658–8663.
29 H. L. Zhu, J. R. Huang, X. W. Zhang, C. Wang, N. Y. Huang, P. Q. Liao and X. M. Chen, *ACS Catal.*, 2021, **11**, 11786–11792.
30 Q. Fan, X. Zhang, X. Ge, L. Bai, D. He, Y. Qu, C. Kong, J. Bi, D. Ding, Y. Cao, X. Duan, J. Wang, J. Yang and Y. Wu, *Adv. Energy Mater.*, 2021, **11**, 2101424.
31 Q. Zhu, C. J. Murphy and L. R. Baker, *J. Am. Chem. Soc.*, 2022, **144**, 2829–2840.
32 X. F. Qiu, H. L. Zhu, J. R. Huang, P. Q. Liao and X. M. Chen, *J. Am. Chem. Soc.*, 2021, **143**, 7242–7246.

33 L. Zhang, X. X. Li, Z. L. Lang, Y. Liu, J. Liu, L. Yuan, W. Y. Lu, Y. S. Xia, L. Z. Dong, D. Q. Yuan and Y. Q. Lan, *J. Am. Chem. Soc.*, 2021, **143**, 3808–3816.
34 L. Hao, Q. Xia, Q. Zhang, J. Masa and Z. Sun, *Chin. J. Catal.*, 2021, **42**, 1903–1920.
35 Y. Yang, Z. Zhang, Z. Zhang, C. Tang, X. Chang and L. Duan, *Chin. J. Chem.*, 2021, **39**, 1281–1287.
36 Y. Wang, X. P. Zhang, H. Lei, K. Guo, G. Xu, L. Xie, X. Li, W. Zhang, U. P. Apfel and R. Cao, *CCS Chem.*, 2022, **4**, 2959–2967.
37 K. Yao, Y. Xia, J. Li, N. Wang, J. Han, C. Gao, M. Han, G. Shen, Y. Liu, A. Seifitokaldani, X. Sun and H. Liang, *J. Mater. Chem. A*, 2020, **8**, 11117–11123.
38 Q. Zhu, X. Sun, D. Yang, J. Ma, X. Kang, L. Zheng, J. Zhang, Z. Wu and B. Han, *Nat. Commun.*, 2019, **10**, 3851.
39 W. Zhang, C. Huang, J. Zhu, Q. Zhou, R. Yu, Y. Wang, P. An, J. Zhang, M. Qiu, L. Zhou, L. Mai, Z. Yi and Y. Yu, *Angew. Chem., Int. Ed.*, 2022, **61**, e202112116.
40 R. Casebolt, K. Levine, J. Suntivich and T. Hanrath, *Joule*, 2021, **5**, 1987–2026.
41 C. Kim, J. C. Bui, X. Luo, J. K. Cooper, A. Kusoglu, A. Z. Weber and A. T. Bell, *Nat. Energy*, 2021, **6**, 1026–1034.
42 R. M. Arán-Ais, F. Scholten, S. Kunze, R. Rizo and B. R. Cuenya, *Nat. Energy*, 2020, **5**, 317–325.
43 H. S. Jeon, J. Timoshenko, C. Rettenmaier, A. Herzog, A. Yoon, S. W. Chee, S. Oener, U. Hejral, F. T. Haase and B. Roldan Cuenya, *J. Am. Chem. Soc.*, 2021, **143**, 7578–7587.
44 J. Timoshenko, A. Bergmann, C. Rettenmaier, A. Herzog, R. M. Arán-Ais, H. S. Jeon, F. T. Haase, U. Hejral, P. Grosse, S. Kühl, E. M. Davis, J. Tian, O. Magnussen and B. R. Cuenya, *Nat. Catal.*, 2022, **5**, 259–267.
45 J. Li, Y. Kuang, Y. Meng, X. Tian, W. H. Hung, X. Zhang, A. Li, M. Xu, W. Zhou, C. S. Ku, C. Y. Chiang, G. Zhu, J. Guo, X. Sun and H. Dai, *J. Am. Chem. Soc.*, 2020, **142**, 7276–7282.
46 K. Jiang, R. B. Sandberg, A. J. Akey, X. Liu, D. C. Bell, J. K. Nørskov, K. Chan and H. Wang, *Nat. Catal.*, 2018, **1**, 111–119.
47 Y. T. Huang, H. Lee, W. D. Li and S. P. Feng, *J. Power Sources*, 2019, **435**, 226801.
48 Y. Wang, Z. Meng, H. Chen, T. Li, D. Zheng, Q. Xu, H. Wang, X. Y. Liu and W. Guo, *J. Mater. Chem. C*, 2019, **7**, 1966–1973.
49 J. Chen, Y. Wang, J. Cao, L. Liao, Y. Liu, Y. Zhou, J. H. Ouyang, D. Jia, M. Wang, X. Li and Z. Li, *Electrochim. Acta*, 2020, **361**, 137036.
50 L. Xu, X. Ma, L. Wu, X. Tan, X. Song, Q. Zhu, C. Chen, Q. Qian, Z. Liu, X. Sun, S. Liu and B. Han, *Angew. Chem., Int. Ed.*, 2022, **61**, e202210375.
51 M. B. Kale, R. A. Borse, A. Gomaa Abdelkader Mohamed and Y. Wang, *Adv. Funct. Mater.*, 2021, **31**, 2101313.
52 T. Kim and G. T. R. Palmore, *Nat. Commun.*, 2020, **11**, 3622.
53 Z. Weng, Y. Wu, M. Wang, J. Jiang, K. Yang, S. Huo, X. F. Wang, Q. Ma, G. W. Brudvig, V. S. Batista, Y. Liang, Z. Feng and H. Wang, *Nat. Commun.*, 2018, **9**, 415.
54 Y. Zhong, X. Kong, Z. Song, Y. Liu, L. Peng, L. Zhang, X. Luo, J. Zeng and Z. Geng, *Nano Lett.*, 2022, **22**, 2554–2560.
55 Z. Chen, T. Wang, B. Liu, D. Cheng, C. Hu, G. Zhang, W. Zhu, H. Wang, Z. J. Zhao and J. Gong, *J. Am. Chem. Soc.*, 2020, **142**, 6878–6883.